c = rotational damping coefficient for governor turbine and gears, 1.2480×10^{-3} m-N-s/rad
c_{cv} = control valve piston friction coefficient, 8.6775×10^{0} N-s/m
c_{gp} = governor piston friction coefficient, 2.7337×10^{0} N-s/m
f_{bsi} = acceleration controller bellows spring preload force, 7.9294×10^{-1} N
f_{cvsi} = control valve spring preload force, 3.8790×10^{1} N
f_{gsi} = governor spring preload force, 2.5308×10^{1} N
g_c = gravitational constant, 3.2200×10^{1} lbm-ft/lbf-s^2
I_t = total mass moment of inertia for turbine, pump, governor, and interconnecting gears, 3.5659×10^{-3} kg-m^2
k_b = acceleration controller bellows spring constant, 4.3081×10^{3} N/m
k_{cvs} = control valve spring constant, 5.2840×10^{2} N/m
k_{gs} = governor spring constant, 6.4038×10^{3} N/m
m_{cvp} = mass of control valve piston, 3.3311×10^{-1} kg
m_{gp} = mass of governor piston, 1.2967×10^{-2} kg
P_a = atmospheric pressure, 1.0135×10^{2} kPa
R = universal gas constant, 2.8747×10^{-1} m^3-kPa/kg-K
$r_{d\,max}$ = maximum working radius of the control valve variable area diaphragm, 2.8569×10^{-2} m
$r_{d\,min}$ = minimum working radius of the control valve variable area diaphragm, 1.5854×10^{-2} m
r_{max} = maximum distance of governor piston center of gravity from axis of rotation, 1.3475×10^{-2} m
r_o = distance of governor piston center of gravity from axis of rotation when the piston is at rest, 7.3456×10^{-3} m
V_{bi} = initial volume of bellows, 3.8730×10^{-6} m^3
V_{ci} = initial volume of control system, 4.9161×10^{-5} m^3
V_{cvi} = initial volume of control valve chamber adjacent to variable area diaphragm, 5.3861×10^{-5} m^3
V_{rv} = volume of reset volume chamber, 5.7356×10^{-5} m^3
V_s = volume of servo chamber, 8.1935×10^{-5} m^3
x_{max} = maximum displacement of control valve piston from rest, 2.9200×10^{-2} m
ω_{gss} = steady-state angular velocity of governor, 5.7450×10^{2} rad/s
ω_{tss} = steady-state angular velocity of turbine, 2.6598×10^{3} rad/s
Δh = enthalpy change of air due to passing through turbine, 3.6519×10^{4} m-N/kg
Δr_d = $r_{d\,max}-r_{d\,min}=1.2714\times10^{-2}$ m

References

[1] Swiecicki, I., 1961, ''Regulation of a Hydraulic Turbine Calculated by Step-By-Step Method,'' ASME J. Basic Eng., **83**, pp. 445–455.
[2] Hutarew, G., 1963, ''Tests on Turbine Governing Systems,'' Water Power, **15**, pp. 243–248.
[3] Parnaby, J., 1964, ''Dynamic and Steady-State Characteristics of a Centrifugal Speed Governor,'' The Engineer, **218**, pp. 879–881.
[4] Schiott, H., and Winther, J., 1965, ''Simulation of a Water Turbine on an Analogue Computer,'' Water Power, **17**, pp. 410–412.
[5] Thorne, D., and Hill, E., 1975, ''Extensions of Stability Boundaries of a Hydraulic Turbine Generating Unit,'' IEEE Trans. Power Appar. Syst., **PAS-94**, pp. 1401–1409.
[6] Hagihara, S., Yokota, H., Goda, K., and Isobe, K., 1979, ''Stability of a Hydraulic Turbine Generating Unit Controlled by P.I.D. Governor,'' IEEE Trans. Power Appar. Syst., **PAS-98**, pp. 2294–2298.
[7] Sanathanan, C., 1986, ''Double Loop Control of a Hydro Turbine Unit,'' Int. Water Power Dam Construction, **38**, pp. 25–27.
[8] Upchurch, E., 1994, ''Determining the Stability of a Pneumatic Turbine Speed Control System Using a Mechanistic Model,'' MS thesis, California State University, Long Beach, Long Beach, CA.
[9] Deshpande, M., and Kar, S., 1981, ''Theoretical Prediction of Characteristics of Certain Flow Control Valves Used in Hydraulic and Pneumatic Systems,'' *Proceedings of the IFAC Symposium on Pneumatic and Hydraulic Components and Instruments in Automatic Control*, May 20–23, 1980, Warsaw, Poland, Pergamon Press, New York.
[10] Benedict, R., and Wyler, J., 1974, ''A Generalized Discharge Coefficient for Differential Pressure Type Fluid Meters,'' ASME J. Eng. Power, **96**, pp. 440–448.

Sonar-Based Wall-Following Control of Mobile Robots

Alberto Bemporad
Automatic Control Laboratory, ETH Zentrum, ETL I24.2, 8092 Zürich, Switzerland

Mauro Di Marco
Alberto Tesi
Dipartimento di Sistemi e Informatica, Università di Firenze, Via di S. Marta 3, 50139 Firenze, Italy;
e-mail: atesi@ingfi1.ing.unifi.it

In this paper, the wall-following problem for low-velocity mobile robots, equipped with incremental encoders and one sonar sensor, is considered. A robust observer-based controller, which takes into account explicit constraints on the orientation of the sonar sensor with respect to the wall and the velocity of the wheels, is designed. The feedback controller provides convergence and fulfillment of the constraints, once an estimate of the position of the mobile robot, is available. Such an estimate is given by an Extended Kalman Filter (EKF), which is designed via a sensor fusion approach merging the velocity signals from the encoders and the distance measurements from the sonar. Some experimental tests are reported to discuss the robustness of the control scheme. [S0022-0434(00)01101-1]

1 Introduction

The ability of following object contours is a basic task in several indoor applications of autonomous mobile robots, such as map building [1,2] and obstacle avoidance [3]. For instance, in unknown environments, when the presence of a new wall is detected, some exploration algorithms command a wall-following in order to collect data on orientation, position, and length of the wall [4].

A sensor fusion integrating data from sensors of distance (e.g., sonars) and velocity (e.g., incremental encoders) is usually employed in the algorithms for following object contours [2,5,6]. Obviously, since reliable sensor fusion is mandatory in practical applications, the robustness of wall-following controllers with respect to sensor constraints is a fundamental issue. For instance, ultrasonic sensors require that the difference between the orientation of the surface of the receiver and the wall is within the beamwidth [7–9], while limits on the supply voltage of the motors impose a constraint on the angular velocity of the wheels.

In this paper we address the problem of designing robust wall-following controllers for low-velocity differential-drive mobile robots. The formulation of the problem includes explicit constraints on the velocity of the wheels and the orientation of the ultrasonic sensors. We propose a wall-following control scheme which ensures both global convergence and constraints fulfillment, once the mobile robot position is available. To deal with practical applications where the robot position can be only estimated, an Extended Kalman Filter (EKF) is added to the controller. Such an EKF provides position and orientation estimates via a sensor fusion approach that integrates the velocity measurements of the

Contributed by the Dynamic Systems and Control Division of THE AMERICAN SOCIETY OF MECHANICAL ENGINEERS. Manuscript received by the Dynamic Systems and Control Division December 2, 1998. Associate Technical Editor: S. D. Fassois.

encoders with the distance measurements of the sonar. Finally, the robustness of the designed observed-based controller is discussed via experimental tests.

The paper is organized as follows. Section 2 presents the wall-following problem. Section 3 contains the main theoretical results on the proposed feedback controller. Section 4 is devoted to the design of the EKF. Section 5 contains experimental results to discuss the performance of the designed observer-based controller, and some concluding comments are drawn in Section 6.

2 Problem Formulation

Consider a differential-drive mobile robot whose coordinates (x,y,θ) in the reference Cartesian space are related by the kinematic equations

$$\begin{cases} \dot{x}=v\cos\theta \\ \dot{y}=v\sin\theta \\ \dot{\theta}=\omega. \end{cases} \tag{1}$$

The velocities v and ω depend on the angular velocities ω_1 and ω_2 of the wheels through the relations

$$\begin{cases} \rho\omega_1=v+e\omega \\ \rho\omega_2=v-e\omega, \end{cases} \tag{2}$$

where ρ and e are the wheel radius and half the wheelbase, respectively. We suppose that the robot is actuated by DC motors and equipped with incremental wheel encoders and a single sonar sensor, on one side of the robot.

We are interested in designing a feedback controller such that the mobile robot moves at a constant speed $v_{\rm des}$ along a wall at a given distance $d_{\rm des}$ from it, as described in Fig. 1. The wall is considered straight and infinite, and is defined by

$$w(x,y)\triangleq(x-x_m)\sin\gamma-(y-y_m)\cos\gamma=0, \tag{3}$$

where the parameters (x_m,y_m) and γ are, respectively, a representative point and the orientation of the wall. Furthermore, let d and r denote the distance of the geometric center C of the mobile robot from the wall and the distance of the sonar from the wall, respectively. It is easy to check that (see Fig. 1)

$$d=(y-y_m)\cos\gamma-(x-x_m)\sin\gamma, \tag{4}$$

$$r=|(x+D_x-x_m)\sin\gamma-(y+D_y-y_m)\cos\gamma|. \tag{5}$$

The quantities D_x and D_y are the components of the line segment joining the sonar and the robot's centerpoint C, i.e.,

$$\begin{cases} D_x=\Delta_y\sin\theta-\Delta_x\cos\theta \\ D_y=-\Delta_y\cos\theta-\Delta_x\sin\theta. \end{cases} \tag{6}$$

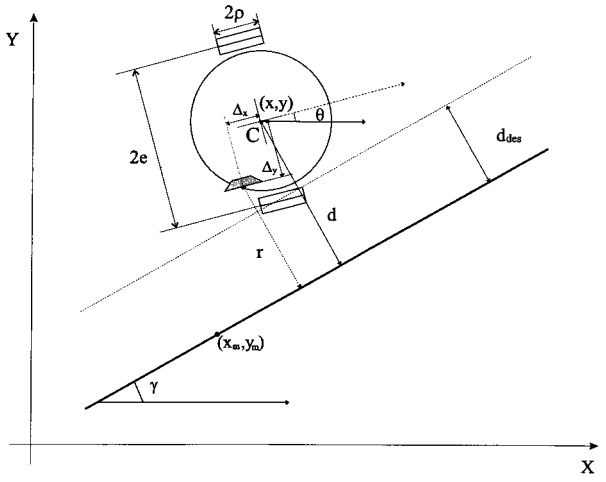

Fig. 1 Wall following problem (WFP)

It is well known that the saturation of the motors may prevent the use of large velocity commands. Also, the encoder and sonar measurements are inevitably corrupted by noise. Moreover, the sonar can collect useful data on the distance from the wall [see Eq. (5)] only when the direction orthogonal to the reflecting surface lies within the beamwidth of the receiver.

Therefore, to ensure robustness of the sought control scheme, we consider explicit constraints in formulating the problem. The motor saturation imposes the velocity constraints

$$|\omega_1|\leqslant\Omega_{\max},\quad |\omega_2|\leqslant\Omega_{\max}, \tag{7}$$

while the beamwidth leads to the orientation constraint

$$|\theta-\gamma|\leqslant\sigma_{\max}. \tag{8}$$

Moreover, it is assumed that $\sigma_{\max}\leqslant\pi/4$, a relation that is satisfied by any commercial ultrasonic device [7–9]. Note that, by exploiting Eq. (2), the constraints (7) can be equivalently rewritten as

$$|v\pm e\omega|\leqslant\rho\Omega_{\max}. \tag{9}$$

(WFP) Wall Following Problem. For the straight and infinite wall described by Eq. (3), determine a feedback control law such that the mobile robot (1) moves at a constant speed $v_{\rm des}$ along the wall at a constant distance $d_{\rm des}$ from it, while satisfying the constraints (8) and (9).

Note that the constraints in (9) imply that $v_{\rm des}$ must be chosen such that

$$v_{\rm des}<\rho\Omega_{\max}. \tag{10}$$

Although in the above problem formulation the wall is assumed to be straight and infinite, the controller scheme developed in the next sections can be succesfully applied also to uneven profiles (see Section 5).

3 Controller Design for the WFP

In this section we propose a solution to the WFP under the assumptions that the coordinates (x,y,θ) are known and the robot dynamics can be neglected. The former assumption will be relaxed in Section 4, while the latter will be discussed in Section 5.

Consider the control law

$$\begin{cases} v=\mu v_{\rm des} \\ \omega=\mu\omega_{\rm des} \end{cases} \tag{11}$$

where

$$\omega_{\rm des}=-\frac{\beta(d-d_{\rm des})}{v_{\rm des}}-(\beta_0+\beta_1|d-d_{\rm des}|)\tan(\theta-\gamma) \tag{12}$$

and μ is selected on-line according to the rule

$$\mu=\max\left\{1,\ \left|\frac{v_{\rm des}\pm e\omega_{\rm des}}{\rho\Omega_{\max}}\right|\right\}^{-1}. \tag{13}$$

Theorem 1. Let $\beta>0$, $\beta_0\geqslant 0$ and $\beta_1\geqslant\beta/(v_{\rm des}\sin\sigma_{\max})$. Then, for every initial condition $(x(0),y(0),\theta(0))$ with $|\theta(0)-\gamma|\leqslant\sigma_{\max}$, the control law (11)–(13) solves the WFP, i.e.,

$$|v(t)\pm e\omega(t)|\leqslant\rho\Omega_{\max} \tag{14}$$

$$|\theta(t)-\gamma|\leqslant\sigma_{\max}, \tag{15}$$

for all $t\geqslant 0$, and

$$d(t)\to d_{\rm des},\quad \dot{d}(t)\to 0,\quad \theta(t)\to\gamma \tag{16}$$

as $t\to\infty$.

Proof. First, we observe that the on-line time-scaling law (13) guarantees that the velocity constraint (14) is always satisfied. In particular, for small values of $\omega_{\rm des}$ we have $\mu=1$, while for larger values it results $\mu<1$.

Exploiting the above fact, we first give the proof under the simplifying assumption that $|v_{des} \pm e\omega_{des}(t)| \leq e\Omega_{max}$ (i.e., $\mu(t)=1$), for all $t \geq 0$. In such a case, supposing without loss of generality $\gamma=0$ and setting $x_1 \triangleq d-d_{des}$, $x_2 \triangleq \dot{d}$, the closed-loop Eqs. (1), (11)–(12) have the form

$$\begin{cases} \dot{x}_1 = x_2 \\ \dot{x}_2 = -\beta x_1 \cos\theta - x_2(\beta_0 + \beta_1 |x_1|). \end{cases} \tag{17}$$

Now, the orientation constraint (8) induces the feasible set $S \triangleq \{(x_1,x_2): |x_2| \leq v_{des} \sin\sigma_{max}\}$. By computing $\dot{x}_2$ for $x_2 = \pm v_{des}\sin\sigma_{max}$ and taking into account for the relation between β and β_1, it can be easily shown that S is invariant, and therefore fulfillment of (15) is ensured.

It remains to prove (16), i.e., the origin is asymptotically stable. This follows from a straightforward application of the LaSalle's theorem to the Lyapunov function

$$V(x_1,x_2) = \beta x_1^2 + \frac{x_2^2}{\sqrt{1-\dfrac{x_2^2}{v_{des}^2}}}.$$

More specifically, taking into account that $\sigma_{max} \leq \pi/4$ and V is proper in S, the following facts can be easily verified [10]: (i) $\dot{V}$ is negative semidefinite in S, (ii) the origin is the largest invariant set contained in $\{\dot{V}=0\} \cap S$.

We now remove the simplifying assumption $\mu=1$. Indeed, it is clear that the asymptotical convergence properties remain unchanged, if a finite time T_f exists such that $\mu(t)=1$ for all $t \geq T_f$. To this purpose, we introduce the new time variable

$$\tau = \int_0^t \mu(\lambda)\, d\lambda. \tag{18}$$

It is straightforward to verify that the same proof of the case $\mu=1$ can be repeated by expressing the dynamics of the system in the new time-reference τ (see [10] for details). In particular, it results

$$\lim_{\tau \to \infty} \omega_{des}(\tau) = 0.$$

Therefore, Eqs. (10) and (13) imply that there exists τ_f such that $\mu(t(\tau))=1$ for all $\tau \geq \tau_f$, where $t(\tau)$ is the inverse of the function defined in (18). In turn, the sought T_f is given by

$$T_f = \int_0^{\tau_f} \frac{1}{\mu(t(\tau))}\, d\tau.$$

Remark 1. Theorem 1 does not provide a specific relation between β_0 and β_1. Indeed, if we let $\beta_0 = \alpha\beta_1$, simulations show that, for small values α, the magnitude of the angular velocity is small enough to avoid sudden rotations of the robot during both steady state and transient operations. On the other hand, simulations also show that larger values of α guarantee better robustness against noise and model uncertainty. Thus, α should be experimentally tuned for the specific application. For our experimental platform, which is described in Section 5, we have chosen $\alpha \in [0.05, 0.1]$ m.

4 Observer Based Controller for the WFP

In practical applications the coordinates (x,y,θ) and the distance d are not known exactly. They must be estimated on the basis of the (noisy) measurements of the sonar and the wheel encoders.

Let $x(k)$, $y(k)$, $\theta(k)$, $\omega(k)$, $v(k)$, $\omega_1(k)$, $\omega_2(k)$, $d(k)$, and $r(k)$ denote the value of x, y, θ, ω, v, ω_1, ω_2, d, and r at time kT_c, respectively, where T_c is the sampling time. Furthermore, let $\overline{\omega_1}(k)$ and $\overline{\omega_2}(k)$ indicate the measurements at time kT_c of the angular velocities ω_1 and ω_2, and $\overline{r}(k)$ the measurements of the distance r.

We use an Extended Kalman Filter (EKF) to obtain an estimate $\hat{x}(k)$, $\hat{y}(k)$, $\hat{\theta}(k)$ of the coordinates, and consequently, via (4), an estimate $\hat{d}(k)$ of the distance d. The EKF will merge the measurements $\overline{\omega_1}(k)$ and $\overline{\omega_2}(k)$ of the incremental encoders with the data $\overline{r}(k)$ of the sonar. To this end, consider the state and velocity measurements vectors

$$X(k) \triangleq [x(k), y(k), \theta(k)]'$$

$$\overline{V}(k) \triangleq [\overline{v}(k), \overline{\omega}(k)]'$$

where $\overline{v}(k) = \rho(\overline{\omega_1}(k) + \overline{\omega_2}(k))/2$ and $\overline{\omega}(k) = \rho(\overline{\omega_1}(k) - \overline{\omega_2}(k))/2e$, and the vector functions

$$F(X(k-1), \overline{V}(k)) \triangleq \begin{bmatrix} x(k-1) + \overline{v}(k) T_c \cos\left(\theta + \dfrac{\overline{\omega}(k) T_c}{2}\right) \\ y(k-1) + \overline{v}(k) T_c \sin\left(\theta + \dfrac{\overline{\omega}(k) T_c}{2}\right) \\ \theta(k-1) + \overline{\omega}(k) T_c \end{bmatrix} \tag{19}$$

$$G(X(k)) \triangleq |(x(k) + D_x - x_m)\sin\gamma - (y(k) + D_y - y_m)\cos\gamma|. \tag{20}$$

Note that Eq. (19) is simply derived using the Simpson's rule for odometric integration, while Eq. (20) is the distance between the sonar sensor and the wall [see Eq. (5)]. Furthermore, let $E_x(k)$ be a random vector [with zero-mean and covariance matrix $Q_x(k)$] which takes into account noise and model uncertainties, and $\xi(k)$ a random variable (with zero-mean and covariance σ_r^2) modeling the noise on the sonar measurements. Combining the above relations, we arrive at the nonlinear model

$$\begin{cases} X(k) = F(X(k-1), \overline{V}(k)) + E_x(k) \\ \overline{r}(k) = G(X(k)) + \xi(k). \end{cases} \tag{21}$$

By applying the standard EKF technique to (21), see e.g. [11], an estimate $\hat{X}(k)$ for $X(k)$ is obtained. Note that (21) includes the encoder measurements $\overline{V}$ as an input, and the sonar measurements $\overline{r}$ as an output. The sensor fusion is obtained by the two-step procedure of EKF [11].

- *Time update*: The velocity measurements $\overline{V}(k)$ are used to update the state in the first equation in (21);
- *Measurement update*: The difference between the estimated r and the measured $\overline{r}$ obtained from the sonar sensor is used to correct the estimate [see second equation in (21)].

The estimate $\hat{X}(k)$ provided by the EKF allows arriving to the following final form of the control law

$$\begin{cases} v = \hat{\mu} v_{des} \\ \omega = -\hat{\mu}\hat{\omega}_{des} \end{cases} \tag{22}$$

where $\hat{\omega}_{des}$ is given by (12) with $\hat{\theta}$ and $\hat{d}$ in place of θ and d, and $\hat{\mu}$ is given by (13) with $\hat{\omega}_{des}$ in place of ω_{des}. Note that $\hat{\theta}$ is the third component of $\hat{X}$, and $\hat{d}$ is evaluated, via Eq. (4), by using the first two components of $\hat{X}$, i.e.,

$$\hat{d} = (\hat{y} - y_m)\cos\gamma - (\hat{x} - x_m)\sin\gamma.$$

Numerical simulations show that the controller (22)+EKF solves the WFP for small starting orientation errors and suitable gains β, β_0 and β_1 and provides a correct estimation of the robot coordinates. The latter result is no longer obtained if only odometric estimation is performed, i.e., $\hat{X}(k) = F(\hat{X}(k-1), \overline{V}(k))$ [10].

5 Experimental Results

The aim of this section is to discuss the enforced assumptions in the WFP, i.e., the robot dynamics can be neglected, the initial conditions are exactly known, the wall is straight and known, with specific reference to the experimental set-up concerning the mobile system ULISSE (Unicycle-Like Indoor Sonar Sensing Ex-

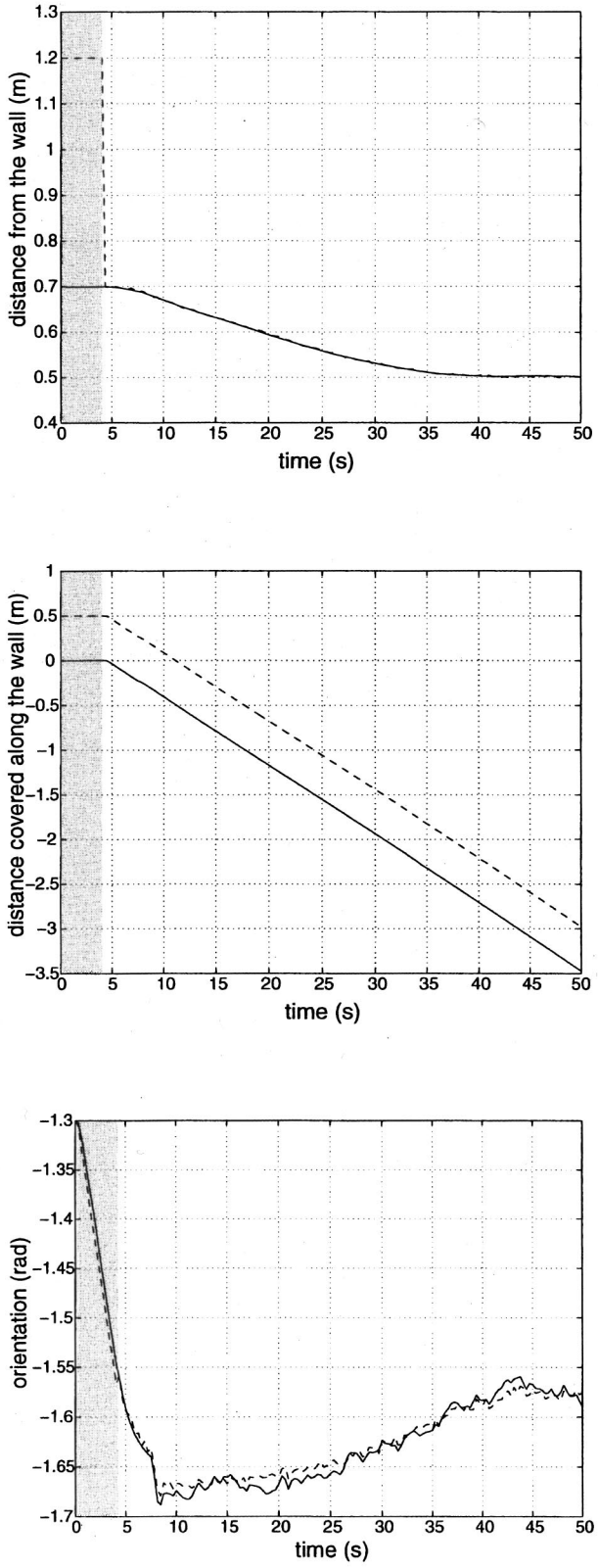

Fig. 2 Evolution of the *x*-coordinate (distance from the wall), *y*-coordinate (distance along the wall) and θ-coordinate: real (solid line) and estimated (dashed-line). In the shadowed zone the EKF is not active.

plorer). ULISSE is a cylindrical robot with two drive wheels ($r = 0.056$ m, $e = 0.189$ m), equipped with two encoders and five sonar sensors. More details on the architecture can be found in [10].

It is a standard rule to neglect robot dynamics in low-velocity indoor applications. Indeed, it turns out that the mechanical and electrical time constants are definitely smaller than the sampling time of the controller. This is the case for the robot ULISSE, since the open-loop time constants are in the range of tenths of milliseconds, while the adopted sampling time $T_c = 0.1$ s. The experimental tests confirm the validity of the assumption since the obtained trajectories satisfactorily agree with the simulated ones (see [10] for more details).

It is well known that the initial conditions are often known only roughly. Therefore, we have investigated the robustness of the control law (22)+EKF with respect to errors on the starting position and orientation of the robot. Figure 2 shows the evolutions of the actual coordinates (solid line) and the corresponding estimates (dashed line) provided by the EKF during a wall following ($x_m = y_m = 0$, $\gamma = 90°$, $d_{\text{des}} = 0.5$ m), when $x(0)$ and $y(0)$ are not known. The control parameters are: $\beta = 0.3\,\text{s}^{-2}$, $\beta_0 = 1.22\,\text{s}^{-1}$, $\beta_1 = 24\,\text{m}^{-1}\,\text{s}^{-1}$, $v_{\text{des}} = 0.08\,\text{ms}^{-1}$. In the shadowed areas the EKF is not active. Note that the initial error on the *y*-coordinate does not decrease. This is due to the fact that the sonar sensor can only provide information on errors directed orthogonally to the direction of the wall. Experimental results also show that errors on the starting orientation up to 10–15 deg (half of the sonar beamwidth) can be tolerated.

We have tested the control scheme in some more complex situations, such as following unknown walls, or following walls with discontinuous profiles. Here, we consider only the case of discontinuous profiles (the case of unknown wall can be found in [10]). In this case, it is possible to use some statistical properties of the EKF to get on-line validation of the environment model. Indeed, if we have a correct parametrization of the environment, it will happen that

$$[\overline{r}(k) - G(\hat{X}(k|k-1))]P_x^{-1}(k|k)[\overline{r}(k) - G(\hat{X}(k|k-1))]^T \leq g \tag{23}$$

where g is a positive threshold value, $P_x(k|k)$ is an estimate of the covariance matrix of the state (used by the EKF) and $\hat{X}(k|k-1)$ is the time update of the EKF. Moreover, $[\overline{r}(k) - G(\hat{X}(k|k-1))]$ will produce incorrelated time series. On the other hand, if the model is wrong, both the aforementioned conditions will fail. Henceforth, by including the test (23) and the correlation test in a higher level controller, it is possible to perform a wall-following task of discontinuous profiles, by alternatively selecting whether to use the environmental model information to get better estimates of the robot position, or to upgrade the model itself. Figure 3

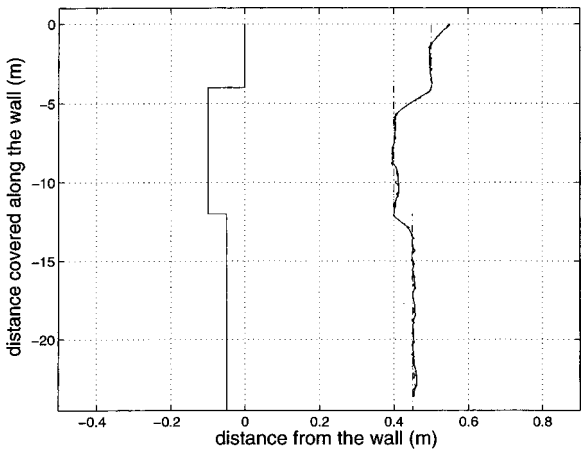

Fig. 3 Following a discontinuous wall: real (solid line) and estimated (dashed-line) robot trajectory

reports an experiment where a discontinuous wall is tracked under the assumption that it is straight. Note how the robot tries to keep the correct distance from the wall, by following its discontinuous profile.

6 Conclusions

In this paper we have considered the problem of wall-following for low-velocity mobile robots. We have described how to design a robust observer-based controller which takes into account constraints on the orientation of the sonar and the velocity of the wheels. The main theoretical result has been the proof of global convergence and constraints fulfillment. From a practical point of view, we have shown how sensor fusion can be achieved by using an EKF, which integrates the measurements of velocity from the encoders and the distance measurements of the sonar. Some experimental results have been reported to discuss the robustness of the designed control scheme.

References

[1] Crowley, J. L., 1985, ''Navigation for an Intelligent Mobile Robot,'' IEEE Trans. Rob. Autom., **RA-1**, No. 1, pp. 31–41.
[2] van Turennout, P., Honderd, G., and van Schelven, L. J., 1992, ''Wall-following Control of a Mobile Robot.'' Proc. IEEE Int. Conf. Robot. Automat., **1**, pp. 280–285.
[3] Latombe, J. C., 1991, *Robot Motion Planning*, KAP, Boston.
[4] Zelinsky, A., 1991, ''Mobile Robot Map Making Using Sonar,'' J. Rob. Syst., **8**, No. 5, pp. 557–577.
[5] Durrant-Whyte, H., 1992, ''Where Am I?,'' Industrial Robot, **21**, No. 2, pp. 11–16.
[6] Holenstein, A. A., and Badreddin, E., 1994, ''Mobile-Robot Positioning Update Using Ultrasonic Range Measurements,'' International Journal of Robotics and Automation, **9**, No. 2, pp. 72–80.
[7] Elfes, A., 1987, ''Sonar-Based Real-World Mapping and Navigation,'' IEEE Trans. Rob. Autom., **RA-3**, No. 3, pp. 249–265.
[8] Bozma, Ö., and Kuc, R., 1991, ''Building a Sonar Map in a Specular Environment Using a Single Mobile Sensor,'' IEEE Trans. Pattern Anal. Mach. Intell., **RA-13**, No. 12, pp. 1260–1269.
[9] McKerrow, P. J., 1993, ''Echolocation—From Range to Outline Segments,'' Rob. Auton. Syst., **11**, pp. 205–211.
[10] Bemporad, A., Di Marco, M., and Tesi, A., 1993, ''Sonar-Based Wall-Following Control of Mobile Robots,'' Research Report DSI-14/97. Dipartimento di Sistemi e Informatica, Firenze.
[11] Mayback, P., 1979, *Stochastic Models—Estimation and Control*, Vol. 1, Academic Press, New York.

Finding Nonconvex Hulls of QFT Templates

Edward Boje
Electrical and Electronic Engineering, University of Natal, Durban, 4041, South Africa
e-mail: boje@eng.und.ac.za

To reduce the computational overhead in quantitative feedback theory (QFT) bound computation, only the (nonconvex) outside edge of a template should be used. This note presents an algorithm to calculate the nonconvex hull with minimum concave radius defined by the feedback system specifications. [S0022-0434(00)01301-0]

1 Introduction

The quantitative feedback theory (QFT) (see [1], for a general reference) is an engineering design methodology for robust control of uncertain systems. Many routine computations and design visualization are currently available in commercial CAD software [2]. To reduce the computational overhead in bound calculation, only the (nonconvex) outside edge of a template should be used. This note presents an algorithm for eliminating interior points of a template (defined in Sec. 2.1), without over-design that results from using a convex hull of the template points. The reduction in the number of template points is achieved by forming a nonconvex hull of the Nichols chart template with a minimum concave radius smaller than the minimum curvature of the feedback system specification at that frequency. If, for example, the plant templates come from multiple system identification experiments, linearization along operating trajectories or gridding of the parameter space, many of the template points will not be required for bound computation.

The results are partially motivated by the algorithm of Rodrigues, Chait, and Hollot [3], which reduces the computational effort required for bound calculation at a given frequency and controller phase. In their algorithm, this is achieved by finding a convex hull of the quadratic inequalities that need to be solved as part of finding a bound numerically. As their algorithm is used at each of a number of discrete phase values, considerable savings can be achieved if the algorithm of this paper is used to eliminate the interior points before calculation of these quadratic inequalities. Of course, the algorithm can be used on its own.

2 Finding Nonconvex Hulls of QFT Templates

2.1 Minimum Radius of a Specification. Robust design on the log-polar plane (Nichols and Inverse Nichols chart) illustrated in Fig. 1 has the great advantage that at any design frequency, ω_i, the controller, $G(j\omega_i)$, only shifts the plant template, $P(j\omega_i) \in \{P(j\omega_i)\}$ (the set of all plants), rather than rotating and scaling it. (This is one of the enduring contributions of the paper of Horowitz and Sidi [4].)

Consider a typical frequency domain sensitivity specification, at a discrete frequency, ω_i,

$$\left|\frac{1}{1+L(\omega_i)}\right| \leq M_i \tag{1}$$

Dropping the subscript, i, and writing the loop transmission in polar form, $L = \mathrm{Re}^{j\theta}$, R is solved from the quadratic inequality,

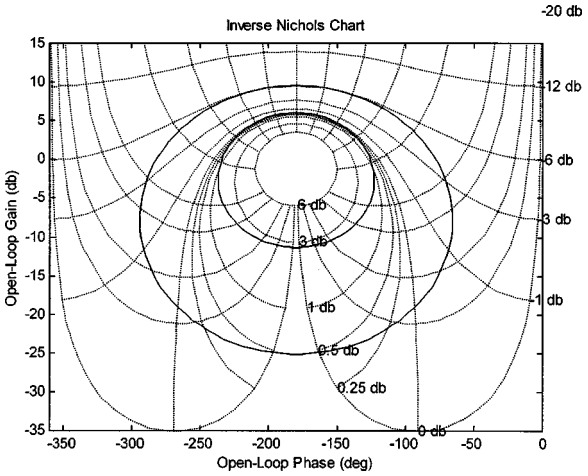

Fig. 1 Inverse Nichols chart showing curvature of M=0 dB and M=−6 dB

Contributed by the Dynamic Systems and Control Division of THE AMERICAN SOCIETY OF MECHANICAL ENGINEERS. Manuscript received by the Dynamic Systems and Control Division December 28, 1998. Associate Technical Editor: E. A. Misawa.